

RESEARCH ARTICLE

Implementation of New Design Concepts to an Axial Compressor and a Case Study with CFD

Taha Gunaydin¹  and Bedii Ozdemir^{1,*} ¹Department of Mechanical Engineering, Istanbul Technical University, Türkiye

Abstract: The present study elaborates on new concepts in designing an axial-flow compressor. With the help of an innovative in-house design code, a rotor design is obtained. Computational fluid dynamics (CFD) was used to explore the level of achievement in the performance of the device with the new attributes. In that, the features including local angle of attack, chord length, camber, and thickness were radially adjusted to fulfill flow rate and pressure head requirements at a specific rotational speed, hub, and tip diameters. At the core of this methodology lies the effective use of a lookup table that interrelates airfoil shapes to their corresponding lift coefficients. The most important outcome was the machine attaining the endurance to stall. Furthermore, the rotor geometry is optimized so that the maximum efficiency coincides with the design point of the device, where a low-pitch air motion with a uniform pressure was observed downstream of the rotor, inducing improved aerodynamic conditions. This leads to the minimization of the tangential stresses, and the level of turbulence remained consistently below 15%, signifying a controlled and efficient flow environment. This research expands the understanding of compressor dynamics and offers a practical design methodology, promising increased operational stability and performance across diverse applications.

Keywords: turbomachinery, computational fluid dynamics (CFD), axial-flow compressor

1. Introduction

The research described here pertains to axial fluid-moving machines, for example, marine and aircraft propellers, inline compressors in gas turbine applications, the frontal fan in turbofan engines, axial fans in IC engine cooling and ventilation applications, hydraulic systems, and the like working on a rotary shaft [1–5]. The axial devices combine the essential features of various fluid-moving devices and, nowadays, they are also having new uses in flow measurement and control in chemical processes, medical devices, and fuel cells [6, 7].

Initially, as the fluid enters an axial-flow-type machine, it comes into contact with the leading edge of the blades. Subsequently, it follows the path along the chord of the blades [8]. Hence, the pitch angle of the blades, which relates to the rate of flow and the static pressure, is a significant factor that directly affects the operation of an axial fan. In contrast to a radial-flow machine, an axial-flow machine minimally alters the direction of the fluid stream before it exits the rotor. As a result, it is anticipated that the inclination angle at the impeller exit, relative to the axis of rotation, will remain small. Even in a vaneless diffuser configuration, it is possible to achieve this characteristic.

In axial-flow-type turbomachines, the impellers are subjected to significant unsteady forces, which can lead to vibrations and fatigue

failure [9]. They are the result of impulsive loading, which is also interrelated with the intermittency of the head curve and rotating instabilities. The number of blades changes the impulsive loading and, hence, increasing it improves the aerodynamic efficiency and the impulsive noise. Enlarging the gap between the casing and the tip of the blade can reduce instabilities observed in the head curve of axial-flow-type machines [10]. However, increased clearance results in the backflow and the tip vortex formation, decreasing the overall efficiency of the fan [11]. The presence of a reversed flow through the impellers adversely affects the overall flow dynamics and, consequently, impairs their performance [12].

The fluid passing through the rotor is in general collected by a downstream ducting, where the flow gradually slows down in the expansion conduit toward the exit. In this process, ensuring a disturbance-free outflow from the rotor is very important for the improved performance of the system. This means minimizing any disruptions or irregularities in the flow as it exits the rotor. Recent research has provided evidence that the use of sweeping blades can aerodynamically redistribute the spanwise front loading, leading to notable improvements in reducing tip leakage and minimizing flow separation [13, 14]. Failing to address these issues could allow the disturbances to persist in the ducting ahead.

The geometric parameters, such as the length of the impeller, have vital importance for determining the pressure gain and efficiency of the machine [15]. Additionally, axial-flow configurations enable significant adjustments in the hub radius, resulting in a diminished impact of centrifugal and Coriolis effects

*Corresponding author: Bedii Ozdemir, Department of Mechanical Engineering, Istanbul Technical University, Türkiye. Email: bozdemir@itu.edu.tr

on pressure rise compared to radial compressors. As a result, the contribution from these effects is smaller in axial-flow configurations. However, there exist other complications in the design processes of the axial fluid-moving devices, where the reverse flow generates a considerable level of turbulence and cavitation [16]. Despite all odds, axial-flow-type turbomachines maintain their strategic importance in comparison to radial-flow machines. This is due to their capability of achieving high-pressure ratios, leading to notably high efficiencies even with very small diameters.

Turbomachinery manufacturers face a strong challenge due to the conflicting design constraints, hindering their ability to venture beyond established and familiar designs [17]. The need for compact machines that are low-noise and energy-efficient, to meet stringent standards for reducing process carbon footprints [18], has been driving designers to explore innovative implementations that have yet to be fully explored. In this regard, recent advancements have demonstrated that the transition from flat impellers to twisted blades, with highly complex topological features [19], has significantly elevated the performance of axial machines to levels previously inconceivable. Among these advancements, multi-objective surrogate-assisted optimization techniques have emerged, demonstrating the potential to enhance the performance of axial fans. Notably, these techniques were employed to optimize fan blade designs, resulting in efficiency improvements under different working conditions [20]. As, for example, the use of the data mining and the free-form deformation techniques presents an innovative optimization procedure for a fan [21], the optimized blade designs have exhibited efficiency gains, reduced static stresses, and insightful sensitivities of design variables.

The proposed investigation will commence by building upon the idea developed by Ozdemir [19] and explore the performance limits for several axial compressors, considering different numbers of blades. We utilize a specialized design concept and programming tool to design a group of axial-flow machines with consistent impeller forms. Our strong in-house numerical turbomachinery design tool ensures a high degree of accuracy, allowing us to produce initial prototypes closely resembling the final design. In this research, we will demonstrate the exploitation of computational fluid dynamics (CFD) analysis [22] in reducing the need for multiple prototypes and extensive experimentation.

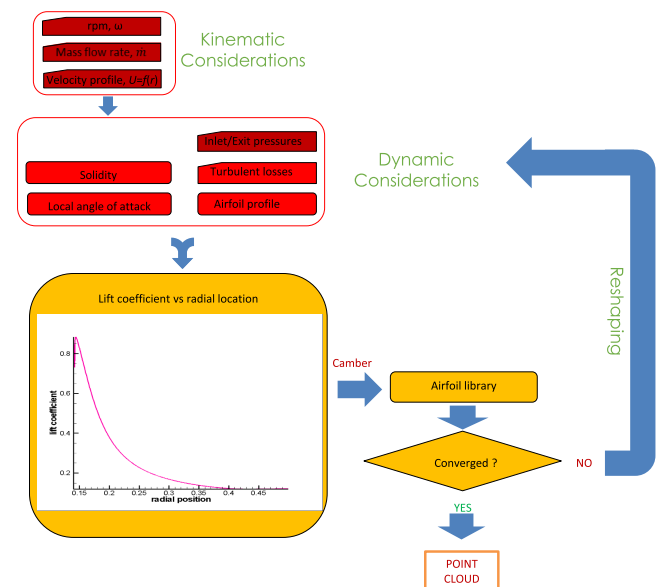
In summary, the key objective of the present investigation is to implement innovative ideas on axial fluid-moving machines to provide low-noise energy efficient operation better than those employed heretofore and, while complying with all of these, make them require no further adjustment throughout their life. The novel design features will be described in the next section.

2. Innovative Design Procedures for Axial Turbomachines

The design of axial-flow-type machines must address unfavorable approach flow conditions, for example, rapid changes in the flow rate since they have significant implications [23]. In an environment of high turbulence, blades can suffer from flow separation, resulting in spatial variations within the rotor and subsequent sections of the ducting. Hence, it is crucial to consider

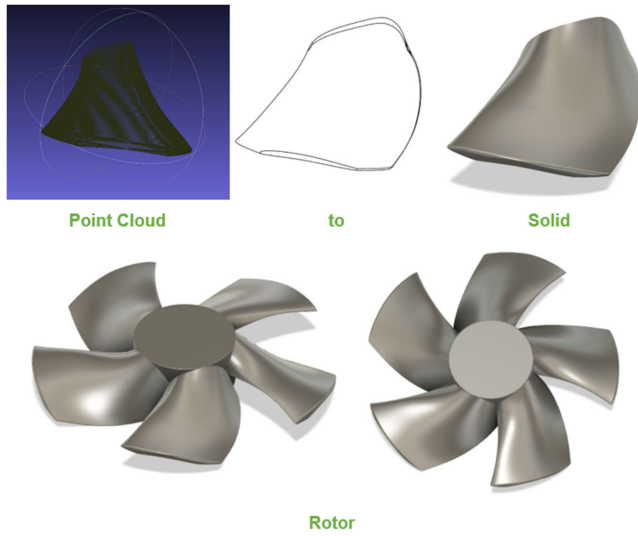
fluctuating as well as average forces on the blades in the design process. These features are effectively taken into account and modifications can be implemented using our in-house code (refer to Figure 1) [19]. The optimization process of the rotor design involves employing mass and momentum balances on a selected cross-sectional area surrounding a generic airfoil. These principles enable the computation of lift and drag forces. These forces serve as essential variables within an iterative scheme. In this iterative procedure, the airfoil's attributes, such as local angle of attack, chord length, camber and thickness, undergo corrections radially. These improvements aim to satisfy the flow rate and pressure head requirements for a given rotational speed, hub, and tip diameters. Central to this approach is the utilization of a lookup table, detailing the correlation between airfoil shapes and lift coefficients. It is also crucial to account for losses stemming from turbulence and cross-flow phenomena occurring along the blade.

Figure 1
The novel design algorithm for axial fluid-moving machine



The software determines the solidity of the rotor and defines the axial velocity distribution along the exit side of the blades. This scheme intends a blade design, characterized by progressively diminishing axial velocities near both the hub and the tip. Hence, the strategy effectively alleviates the tip vortices, which form in shear layers at the extremities of the blade, consequently resulting in a reduction of tip noise. This innovative configuration, characterized by lower velocities at the tip and hub of the blade, prompts an inward radial-flow downstream of the rotor. This, in turn, engenders a notable enhancement in energy efficiency and concurrently diminishes the acoustic emissions associated with the exhaust process into the tail ducting [19]. The rotor geometry was described by a point cloud file and a text file, which consists of the solidity information and some other relevant data. The progress of the design from the point cloud to the 3D rotor geometry is shown in Figure 2.

Figure 2
Design procedures from point cloud to solid model



3. Transport Equations and CFD Analyses

We first need to know if the flow in the machine is compressible or incompressible for the given operating conditions. Using the compressible flow relation [24]

$$\Delta\rho/\rho = (1 + \Delta p/p)^{1/\gamma} - 1 \quad (1)$$

where γ being the heat capacity ratio, it can be demonstrated that the range of Δp studied in this investigation (the pressure heads varying as $\Delta p = 120 - 480$ Pa) corresponded to a relative change of density ($\Delta\rho/\rho$) smaller or equal to 2%. Hence, the flow was considered as incompressible. The transport equations were introduced in the following without any further elaboration, as one can refer to the works cited in reference [22]. Using the Reynolds decomposition.

$$u = \bar{u} + u' \quad (2)$$

(where \bar{u} and u' refer the averaged and fluctuating components of the velocity, respectively, with $\bar{u}' \equiv 0$), the steady flow equations for mass and momentum are written as

$$\nabla \cdot \bar{u} = 0 \quad (3)$$

and

$$\nabla \cdot (\bar{u}\bar{u}) = -\frac{1}{\rho}\nabla\bar{p} + \nabla \cdot \frac{\mu}{\rho}(\nabla\bar{u} + \nabla\bar{u}^T) \quad (4)$$

where \bar{p} and ρ denote the average pressure and density, respectively, and μ refers to the dynamic viscosity. The Reynolds-averaged Navier-Stokes formalism was employed with the Shear Stress Transport (SST) k - ω turbulence closure model for the turbulent kinetic energy (k) [25],

$$u_j \frac{\partial k}{\partial x_j} = \tau_{ij} \frac{\partial u_i}{\partial x_j} - \beta^* k \omega + \frac{\partial}{\partial x_j} \left[(v + \sigma_k \nu_T) \frac{\partial k}{\partial x_j} \right] \quad (5)$$

and for the dissipation rate (ω),

$$u_j \frac{\partial \omega}{\partial x_j} = \frac{\lambda}{\nu_T} \tau_{ij} \frac{\partial u_i}{\partial x_j} - \beta \omega^2 + \frac{\partial}{\partial x_j} \left[(v + \sigma_\omega \nu_T) \frac{\partial \omega}{\partial x_j} \right] + 2(1 - F_1) \sigma_{\omega 2} \frac{1}{\omega} \frac{\partial k}{\partial x_i} \frac{\partial \omega}{\partial x_i} \quad (6)$$

The constants ϕ are calculated from the constants ϕ_1 and ϕ_2 as follows:

$$\phi = \phi_1 F_1 + \phi_2 (1 - F_1) \quad (7)$$

with functions F_1 and F_2 defined as

$$F_1 = \tanh \left\{ \left\{ \min \left[\max \left(\frac{\sqrt{k}}{\beta^* \omega y}, \frac{500\nu}{y^2 \omega} \right), \frac{4\sigma_{\omega 2} k}{CD_{k\omega} y^2} \right] \right\}^4 \right\} \quad (8)$$

$$F_2 = \tanh \left[\left[\max \left(\frac{2\sqrt{k}}{\beta^* \omega y}, \frac{500\nu}{y^2 \omega} \right) \right]^2 \right] \quad (9)$$

with

$$CD_{k\omega} = \max \left(2\rho\sigma_{\omega 2} \frac{1}{\omega} \frac{\partial k}{\partial x_i} \frac{\partial \omega}{\partial x_i}, 10^{-10} \right) \quad (10)$$

the constants for the SST model are given as [25]

$$\alpha_1 = \frac{5}{9}, \quad \alpha_2 = 0.44 \quad (11)$$

$$\beta_1 = \frac{3}{40}, \quad \beta_2 = 0.0828 \quad (12)$$

$$\beta^* = \frac{9}{100} \quad (13)$$

$$\sigma_{k1} = 0.85 \quad \text{and} \quad \sigma_{k2} = 1 \quad (14)$$

$$\sigma_{\omega 1} = 0.5 \quad \text{and} \quad \sigma_{\omega 2} = 0.856 \quad (15)$$

$$\lambda_1 = \frac{\beta_1}{\beta^*} - \frac{\sigma_{\omega 1} \kappa^2}{\sqrt{\beta^*}} \quad \text{and} \quad \lambda_2 = \frac{\beta_2}{\beta^*} - \frac{\sigma_{\omega 2} \kappa^2}{\sqrt{\beta^*}} \quad (16)$$

$$\kappa = 0.41 \quad (17)$$

4. Numerical Solution Procedures

For computational efficiency, the rotating and the non-rotating regions of the flow domain were separated by using multiple reference frame techniques [26] where the velocity components within the rotary part were written in a rotating reference frame [27].

A mesh check was performed to demonstrate the independence of the volumetric flow rate (Q) from the mesh element count. The study revealed that increasing the number of elements did not significantly alter the volumetric flow rate, while it did lead to an increase in computation time. The graphical representation of the mesh study can be observed in Figure 3. The computational domain for the

Figure 3
Volumetric flow rate independence from mesh size

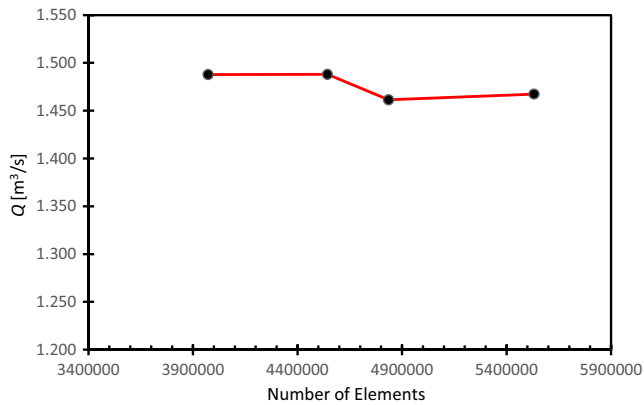
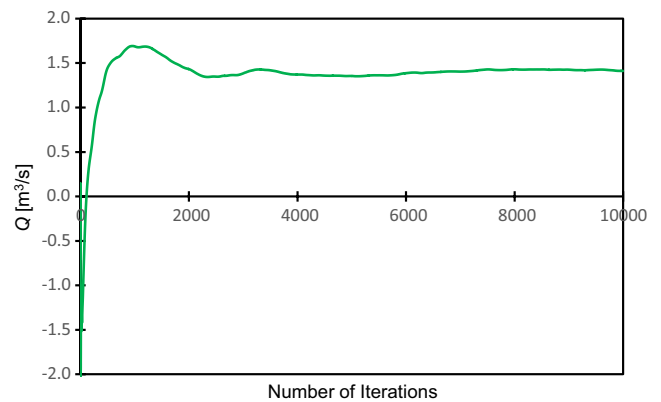


Figure 4
The outlet flow rate at 360 Pa versus the number of iterations (shown up to 10,000 iterations)



present axial-flow machine underwent discretization into a mesh containing a sufficient number of cells (4,390,000 cells). This choice struck a balance between accuracy, computational cost, and numerical stability, providing sufficient resolution in critical regions characterized by sharp velocity gradients such as the inlet-outlet regions, and the interface between rotating and stationary elements, and walls [28].

The simulations were conducted using the OpenFOAM open-source code [29], which employs the finite volume method and is well-suited for modeling rotational flows in intricate geometries. For the velocities, a flux-corrected Neumann boundary condition was used at the inlet and outlet: To ensure a streamlined approach flow into the compressor, the inlet velocities were taken normal to the sphere attached to the diffuser lip. The corrected boundary condition enhances the stability of the simulation since it aligns the velocities with the pressure on the boundaries and offers a more accurate description of the physical behavior than the zero-gradient condition. Regarding the pressure, a prescribed value (Dirichlet boundary condition) [30] was defined at the outlet; a value of small suction pressure (almost zero) was used at the inlet. All wall surfaces were described with the no-slip condition.

The SIMPLE algorithm was utilized for the velocity-pressure coupling. In pursuit of numerical stability and accuracy, second-order discretization schemes are employed in various derivative operations, such as Laplacian terms (Gauss linear corrected), divergence computation (using Gauss linear), gradient computation (Gaussian integration with linear interpolation), and convective terms (Gauss linear upwind). First-order schemes are also incorporated to enhance overall stability. The calculations were performed by parallelizing 16 cores of an Intel Xeon processor.

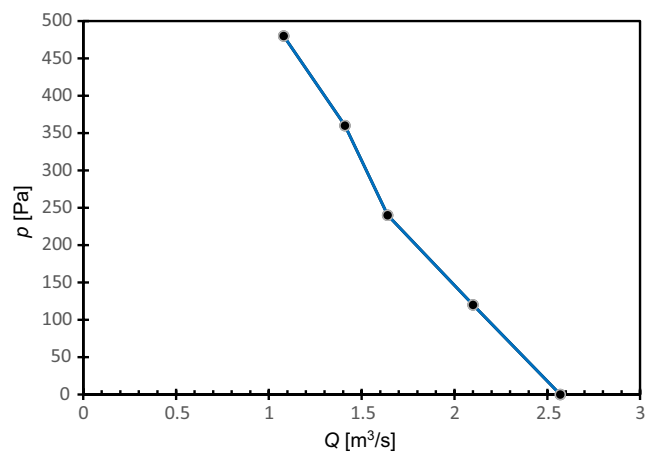
5. Results and Discussion

The speed of the fan was fixed at 1870 rpm. To build the performance curves, the simulations were performed for five pressure loads, 0, 120, 240, 360, and 480 Pa. The volumetric flow rate through the fan converged after 10,000 iterations with the residuals less than 10^{-4} . The change in flow rate with the iterations is shown in Figure 4. Table 1 shows the resulting flow rates for different outlet pressures and the corresponding $p-Q$ trend is given in Figure 5.

Table 1
Flow rates versus pressure load

Outlet pressure [Pa]	Flow rate [m^3/s]
0	2.54
120	2.10
240	1.64
360	1.41
480	1.08

Figure 5
Characteristic curve of the fan



It can be deduced from the characteristic curve that the fan did not exhibit any stall characteristics for the pressure loads within the region where the present calculations were performed. This indicates that the present compressor design demonstrates a strong immunization to stall.

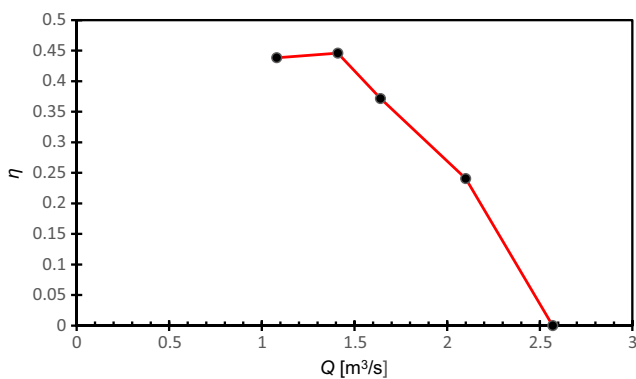
For each operating point, using the total moments acting on the blades, the efficiencies (η) were calculated using the relation,

$$\eta = \frac{P_{\text{output}}}{P_{\text{input}}} = \frac{\Delta p Q}{M_{\text{total}} \Omega} \quad (18)$$

where M_{total} is the total moment acting on the fan in the flow direction and Ω is the angular speed. The efficiency is given in Figure 6 and it is clear that the best efficiency occurs at the operating point where the pressure difference was 360 Pa. The decrease in efficiency appears faster toward the higher flow rates (i.e., toward the low-pressure loads). This is one of the features introduced by the new design concepts and is a very favorable characteristic that the maximum efficiency point coincides with the design point.

Figure 6

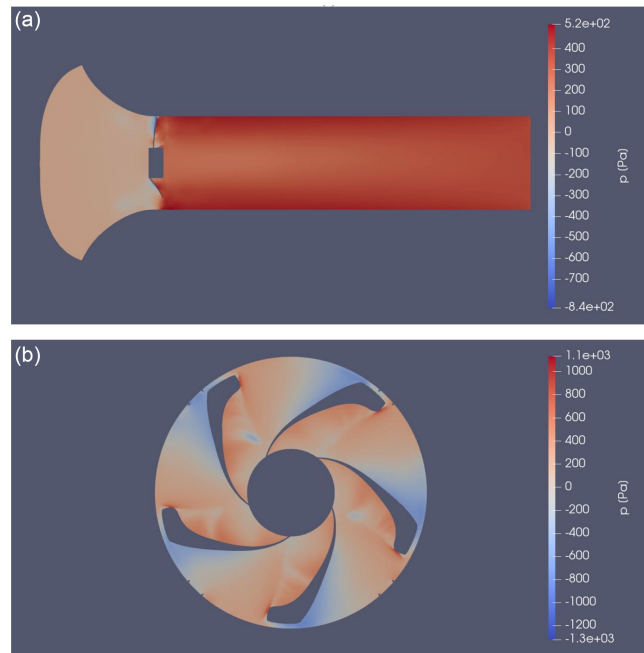
Efficiency of the fan over different operating points



The pressure distribution for the best efficiency point (360 Pa) is given in Figure 7. As expected, the pressure increases from the inlet (the lowest) value at the upstream side of the compressor and jumps to the highest value on the load side: The pressure appears to be uniformly distributed on the exhaust duct downstream of the

Figure 7

Pressure distribution at the best efficiency point (360 Pa): (a) on the plane along the rotor axis and (b) on the plane perpendicular to the rotor axis

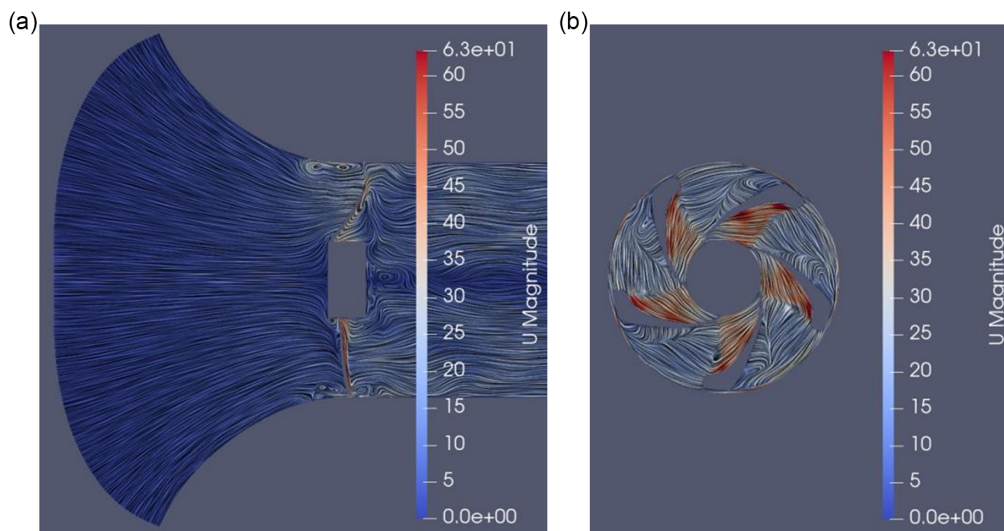


rotor. The uniformity is achieved in a very short distance along the rotor axis. It should also be noted that there is almost no flow leakage to the suction side.

The streamlines at the best efficiency point (360 Pa) are presented in Figure 8, and it can be noticed that the pitch of the streamlines across the tunnel is higher for the higher pressure

Figure 8

Streamlines for the best efficiency point (360 Pa): (a) 2D presentation of the streamlines on the plane along the rotor axis and (b) 2D presentation of the streamlines on the plane perpendicular to the rotor axis

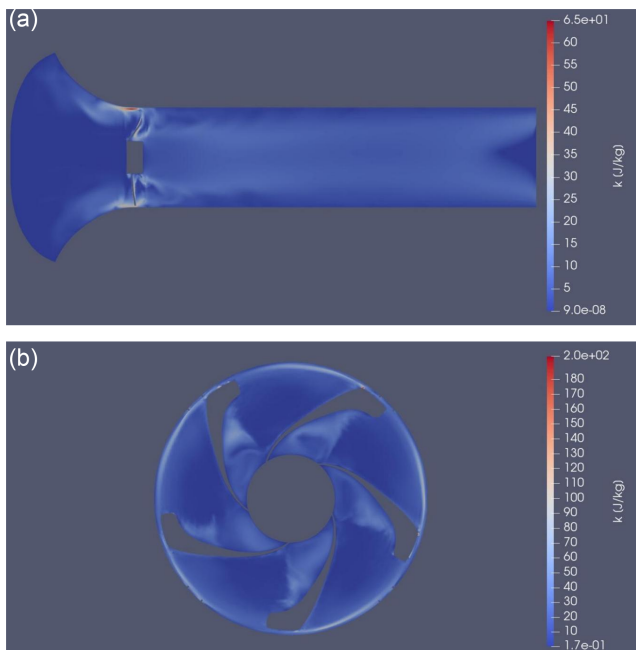


loads. From a design standpoint, the low pitch means that less energy is consumed by the work of the tangential stresses and this results in a higher efficiency.

The axial component of the velocity values is larger on the load side of the compressor. Indeed, this was a very favorable feature revealing that no significant swirling motion existed in the plane perpendicular to the rotor axis. This suggests that the blades do not chew up the air and, hence, do not waste any mechanical energy to drive the rotational motion inside the downstream ducting.

The turbulent kinetic energy distribution at the best efficiency point (360 Pa) is given in Figure 9. It is apparent that the turbulence reached the maximum values on the pressure side, immediately next to the walls of the rotor, where a significant momentum transfer occurred in the flow. However, even in the zone with the highest turbulence, the turbulent intensity always remained lower than 15%.

Figure 9
Turbulent kinetic energy distribution at the best efficiency point (360 Pa): (a) on the plane along the rotor axis and (b) on the plane perpendicular to the rotor axis



6. Conclusions

In this work, innovative concepts and a new in-house code were introduced in designing an axial compressor. Features were applied in a test case and, by using numerical simulations, they were assessed to investigate their effect on the characteristics of the new designs. The computations showed that the new concepts can lead to a compressor design with a strong resistance to stall. The efficiency was observed to increase toward the high-pressure loads, and its maximum occurred exactly at the design point of the device. It seemed that the machine delivered a flow with almost no tip leakage and uniform pressure to the region downstream of the rotor. The streamlines portrayed a low-pitch air motion, indicating that the work of the tangential stresses was almost negligible. It should also be pointed out that the turbulence intensity observed

on the pressure side always remained lower than 15%. This explains the higher efficiency observed.

Ethical Statement

This study does not contain any studies with human or animal subjects performed by any of the authors.

Conflicts of Interest

The authors declare that they have no conflicts of interest to this work.

Data Availability Statement

Data available on request from the corresponding author upon reasonable request.

Author Contribution Statement

Taha Gunaydin: Conceptualization, Software, Validation, Formal analysis, Investigation, Data curation, Writing – original draft, Writing – review & editing, Visualization; **Bedii Özdemir:** Conceptualization, Methodology, Validation, Formal analysis, Resources, Data curation, Writing – original draft, Writing – review & editing, Visualization, Supervision, Project administration.

References

- [1] Bowerman, R. D. (1956). The design of axial flow pumps. *Transactions of the American Society of Mechanical Engineers*, 78(8), 1723–1734. <https://doi.org/10.1115/1.4014163>
- [2] Carlton, J. S. (2007). *Marine propellers and propulsion, (second edition)*. UK: Butterworth-Heinemann.
- [3] Hunt, A. G. (2000). *High efficiency, axial flow fan for use in an automotive cooling system (U.S. Patent No. 6065937)*. U.S. Patent and Trademark Office.
- [4] Sforza, P. M. (2017). *Theory of aerospace propulsion. (second edition)*. UK: Butterworth-Heinemann.
- [5] Soares, C. (2014). *Gas turbines: A handbook of air, land and sea applications*. UK: Butterworth-Heinemann.
- [6] Culjat, M., Singh, R., & Lee, H. (2012). *Medical devices: Surgical and image-guided technologies*. USA: John Wiley & Sons.
- [7] Gee, M. K. (2000). Air management subsystems. In S. Chalk (Ed.), *Progress report for fuel cell power systems* (pp. 127–143). U. S. Department of Energy.
- [8] Castagnarò, S. (2018). Aerodynamic design of low-speed axial-flow fans: A historical overview. *Designs*, 2(3), 20. <https://doi.org/10.3390/designs2030020>
- [9] Srinivas, G., Raghunandana, K., & Satish, S. B. (2018). Axial-flow compressor analysis under distorted phenomena at transonic flow conditions. *Cogent Engineering*, 5(1), 3638–3653. <https://doi.org/10.1080/23311916.2018.1526458>
- [10] Kan, N., Liu, Z., Shi, G., & Liu, X. (2021). Effect of tip clearance on helico-axial flow pump performance at off-design case. *Processes*, 9(9), 1653. <https://doi.org/10.3390/pr9091653>
- [11] Moghadam, S. M. A., Meinke, M., & Schröder, W. (2019). Analysis of tip-leakage flow in an axial fan at varying

- tip-gap sizes and operating conditions. *Computers & Fluids*, 183, 107–129.
- [12] de Ruyck, J., Hirsch, Ch., & Segaert, P. (1990). Secondary flow and radial mixing predictions in axial compressors, secondary flows in turbomachines. In *AGARD Conference Proceedings*, 469, 1–19.
- [13] Yang, A., Tang, T., Zhang, H., & Chen, K. (2009). Effect of swept blade on performance of a small size axial fan. In *Fluid Machinery and Fluid Mechanics: 4th International Symposium*, 279–284.
- [14] Ye, X., Fan, F., Zhang, R., & Li, C. (2019). Prediction of performance of a variable-pitch axial fan with forward-skewed blades. *Energies*, 12(12), 2353. <https://doi.org/10.3390/en12122353>
- [15] Huang, C. H., & Gau, C. W. (2012). An optimal design for axial-flow fan blade: Theoretical and experimental studies. *Journal of Mechanical Science and Technology*, 26(2), 427–436.
- [16] Liu, B., Qiu, Y., An, G., & Yu, X. (2019). Experimental investigation of the flow mechanisms and the performance change of a highly loaded axial compressor stage with/without stator hub clearance. *Applied Sciences*, 9(23), 5134. <https://doi.org/10.3390/app9235134>
- [17] Dawes, W. N., Dhanasekaran, P. C., Demargne, A. A. J., Kellar, W. P., & Savill, A. M. (2001). Reducing bottlenecks in the CAD-to-Mesh-to-Solution cycle time to allow CFD to participate in design. *Journal of Turbomachinery*, 123(3), 552–557.
- [18] Energy Efficiency Opportunities Act. (2014). <https://www.legislation.gov.au/C2006A00031/latest/text>
- [19] Ozdemir, I. B. (2015). A novel methodology for designing axial-type flow machines. *Fluids Group Report FGR-2015-1*.
- [20] Kong, C., Wang, M., Jin, T., & Liu, S. (2023). The blade shape optimization of a low-pressure axial fan using the surrogate-based multi-objective optimization method. *Journal of Mechanical Science and Technology*, 37(1), 179–189.
- [21] Adjei, R. A., Fan, C., Wang, W. Z., & Liu, Y. Z. (2021). Multidisciplinary design optimization for performance improvement of an axial flow fan using free-form deformation. *Journal of Turbomachinery*, 143(1), 011003.
- [22] Ferziger, J. H., & Peric, M. (2002). *Computational methods for fluid dynamics*. German: Springer.
- [23] Oro, J. M. F., Ballesteros-Tajadura, R., Marigorta, E. B., Diaz, K. M. A., & Morros, C. S. (2008). Turbulence and secondary flows in an axial flow fan with variable pitch blades. *Journal of Fluids Engineering*, 130(4), 041101.
- [24] Shapiro, A. H. (1954). *The dynamics and thermodynamics of compressible fluid flow*. USA: The Roland Press.
- [25] Menter, F. (2012). Zonal two equation k-w turbulence models for aerodynamic flows. In *23rd Fluid Dynamics, Plasmadynamics, and Lasers Conference*, 2906.
- [26] Franzke, R., Sebben, S., Bark, T., Willeon, E., & Broniewicz, A. (2019). Evaluation of the multiple reference frame approach for the modelling of an axial cooling fan. *Energies*, 12(15), 2934. <https://doi.org/10.3390/en12152934>
- [27] Gullberg, P., Löfdahl, L., Adelman, S., & Nilsson, P. (2009). A correction method for stationary fan CFD MRF models. In *SAE World Congress & Exhibition*.
- [28] Jakirlic, S., Hanjalic, K., & Tropea, C. (2002). Modeling rotating and swirling turbulent flows: A perpetual challenge. *ALAA Journal*, 40(10), 1984–1996.
- [29] Weller, H. G., Tabor, G., Jasak, H., & Fureby, C. (1998). A tensorial approach to computational continuum mechanics using object-oriented techniques. *Computers in Physics*, 12(6), 620–631. <https://doi.org/10.1063/1.168744>
- [30] Kunz, P., Hirschler, M., Huber, M., & Nieken, U. (2016). Inflow/outflow with Dirichlet boundary conditions for pressure in ISPH. *Journal of Computational Physics*, 326, 171–187.

How to Cite: Gunaydin, T., & Ozdemir, B. (2024). Implementation of New Design Concepts to an Axial Compressor and a Case Study with CFD. *Archives of Advanced Engineering Science*, 2(4), 198–205. <https://doi.org/10.47852/bonviewAAES32021273>

Appendix

Nomenclature

ρ Density
 p Pressure
 γ Specific heat ratios
 u Velocity
 \bar{u} Time-averaged velocity
 u' Fluctuating velocity
 μ Dynamic viscosity
 k Turbulent kinetic energy

x_j Coordinate variable
 ω Turbulent dissipation rate
 η Efficiency
 P Power
 Q Volumetric flow rate
 Ω Angular speed
 τ_{ij} Turbulent stress tensor
 ν Kinematic viscosity
 ν_T Eddy viscosity
 y Shortest distance to a wall